Research Square

Preprints are preliminary reports that have not undergone peer review.
They should not be considered conclusive, used to inform clinical practice,
or referenced by the media as validated information.

Ilmenite-Derived TiO_2 nanoparticles supported on sugarcane bagasse biomass carbon for photocatalytic degradation of sulfamethoxazole

Thu Hang Nguyen Thi
Joint Vietnam-Russia Tropical Science and Technology Research Center
Phuong Anh Cao
Joint Vietnam-Russia Tropical Science and Technology Research Center
Trung Hieu Vu
Joint Vietnam-Russia Tropical Science and Technology Research Center
Duc Anh Nguyen
Joint Vietnam-Russia Tropical Science and Technology Research Center
Irina Alexandrovna Kurzina
National Research Tomsk State University
Hoai Phuong Nguyen Thi
hoaiphuong1978@gmail.com

Joint Vietnam-Russia Tropical Science and Technology Research Center

Research Article

Keywords: Ilmenite valorization, TiO_2/carbon composite, biomass-derived carbon, photocatalytic degradation, sulfamethoxazole removal

Posted Date: June 22nd, 2026

DOI: https://doi.org/10.21203/rs.3.rs-9877487/v1

License: This work is licensed under a Creative Commons Attribution 4.0 International License.
Read Full License

Additional Declarations: No competing interests reported.

Ilmenite-Derived TiO_2 nanoparticles supported on sugarcane bagasse biomass carbon for photocatalytic degradation of sulfamethoxazole

Thu Hang Nguyen Thi[1,2], Phuong Anh Cao[1], Trung Hieu Vu[1], Duc Anh Nguyen[1], Irina Alexandrovna Kurzina[3], Hoai Phuong Nguyen Thi[1,*]

[1]*Joint Vietnam-Russia Tropical Science and Technology Research Center, 63 Nguyen Van Huyen Street, Ha Noi, Vietnam*

[2]*Graduate University of Sciences and Technology, Vietnam Academy of Science and Technology, 18 Hoang Quoc Viet, Nghia Do, Ha Noi*

[3]*Department of Physical and Colloid Chemistry, National Research Tomsk State University, 36 Lenin Ave., Tomsk 634050, Russia*

Abstract

This study reports a sustainable TiO_2/SBAC composite prepared from two low-cost resources, ilmenite ore as the TiO_2 precursor and sugarcane bagasse as the biomass carbon source, for adsorption-assisted photocatalytic degradation of sulfamethoxazole (SMX) in water. Ilmenite-derived TiO_2 was immobilized on sugarcane-bagasse-derived activated carbon through an in-situ deposition route, producing a hybrid material that combines porous adsorption sites with photocatalytic activity. Structural characterization confirmed that pristine SBAC possessed a layered porous carbon framework, while TiO_2/SBAC showed TiO_2 nanoparticles anchored on the carbon surface. XRD revealed anatase and rutile TiO_2 phases in the composite, and FTIR indicated oxygen-containing functional groups and Ti–O-related vibrations. The TiO_2/SBAC composite retained a mesoporous structure with a BET surface area of 339.39 $m^2\ g^{-1}$ and exhibited an optical band gap of 3.18 eV. In SMX removal tests, direct photolysis was negligible, with only 5.45% removal after 60 min. SBAC showed strong dark adsorption, while TiO_2 exhibited effective photocatalytic degradation. The TiO_2/SBAC

composite achieved the highest SMX removal efficiency of 99.46% within 60 min under simulated solar irradiation, demonstrating a clear adsorption–photocatalysis synergy. Kinetic analysis showed that the Elovich model gave the best fit (R^2 = 0.984), indicating removal on heterogeneous active sites. Scavenger experiments identified $\bullet O_2^-$ as the dominant reactive species, followed by h^+ and •OH. TOC decreased from 4.67 to 0.03 mg L^{-1}, corresponding to near-complete mineralization. The catalyst also retained about 86–87% efficiency after five cycles, confirming acceptable stability. These results demonstrate that ilmenite-derived TiO_2 supported on sugarcane bagasse biomass carbon is a promising low-cost photocatalyst for antibiotic-contaminated water treatment.

Keywords: Ilmenite valorization, TiO_2/carbon composite, biomass-derived carbon, photocatalytic degradation, sulfamethoxazole removal

Introduction

The continuous release of antibiotic residues into aquatic environments has become an important environmental concern because these compounds can persist at trace levels, disturb microbial communities, and contribute to the dissemination of antibiotic resistance [1, 2]. Among them, sulfamethoxazole (SMX), a representative sulfonamide antibiotic, is widely used in human medicine, veterinary treatment, and aquaculture [3, 4]. Owing to its incomplete metabolism and partial removal in conventional wastewater treatment plants, SMX has been frequently detected in surface water, groundwater, municipal effluents, hospital wastewater, and agricultural runoff. Even at low concentrations, the long-term presence of SMX may exert selective pressure on microorganisms, promoting the spread of antibiotic-resistant bacteria and resistance genes. Therefore, the development of efficient, low-cost, and environmentally sustainable technologies for SMX removal from water remains a critical research priority [5-7]. Various treatment processes, including adsorption [8], membrane filtration [9], biodegradation [10], ozonation [11], Fenton oxidation [12], persulfate activation [13], and

photocatalysis [14], have been investigated for the removal of SMX from aqueous systems. Among these approaches, semiconductor photocatalysis is particularly attractive because it can degrade organic contaminants by generating reactive oxygen species under light irradiation. Titanium dioxide (TiO_2) remains one of the most studied semiconductor photocatalysts for environmental remediation owing to its chemical stability, low toxicity, abundance, and strong oxidative ability. Under light excitation, TiO_2 generates electron-hole pairs that can react with oxygen and water to form reactive oxygen species capable of degrading organic contaminants. However, pristine TiO_2 has several intrinsic drawbacks, including a wide band gap, limited visible-light absorption, rapid recombination of photogenerated charge carriers, and relatively weak adsorption toward some organic pollutants [15]. These limitations reduce the effective utilization of solar energy and restrict the practical performance of TiO_2 in wastewater treatment. Recent studies have therefore focused on modifying TiO_2 through morphology control, heterojunction construction, elemental doping, defect engineering, and coupling with porous carbonaceous supports. Carbon-supported TiO_2 composites are particularly attractive because the carbon phase can simultaneously act as an adsorbent, dispersing matrix, and electron-transfer mediator. Biochar or biomass-derived carbon generally contains porous channels, aromatic domains, and oxygen-containing functional groups, which can enhance SMX adsorption through pore filling, π-π interactions, hydrogen bonding, and electrostatic attraction. When TiO_2 nanoparticles are immobilized on biomass carbon, particle aggregation can be suppressed, interfacial contact with pollutants can be improved, and photogenerated electrons may be transferred from TiO_2 to carbon domains, thereby reducing electron-hole recombination [16-18]. Previous studies on TiO_2/biochar-based composites have demonstrated that coupling adsorption and photocatalytic oxidation can significantly improve SMX removal compared with either adsorption or photocatalysis alone [14]. This confirms the importance of designing hybrid materials in which pollutant enrichment and oxidative degradation occur cooperatively.

Sugarcane bagasse is an abundant lignocellulosic by-product generated from the sugar industry. It is mainly composed of cellulose, hemicellulose, and lignin, making it suitable for conversion into porous biomass carbon through carbonization and activation [19, 20]. Valorization of sugarcane bagasse into functional carbon materials is environmentally meaningful because it reduces agricultural waste and provides a low-cost support for water-treatment catalysts. Sugarcane bagasse-derived carbon can offer high surface area, hierarchical porosity, surface functional groups, and structural stability, all of which are beneficial for adsorption-assisted photocatalytic systems [21]. In TiO_2/carbon composites, such a support can improve the dispersion of TiO_2, increase accessible active sites, facilitate mass transfer, and promote the adsorption of sulfamethoxazole molecules near photocatalytic centers [22]. This approach is consistent with the concept of waste-to-resource conversion and supports the development of circular materials for environmental remediation. In addition to selecting a sustainable carbon source, the titanium precursor is another important factor affecting the economic and environmental feasibility of TiO_2 photocatalysts. Most TiO_2-based materials are prepared from commercial titanium salts or alkoxides, which may increase synthesis cost and reduce scalability [23, 24]. Ilmenite, a naturally abundant $FeTiO_3$ mineral, is an important titanium resource and has been investigated as a low-cost precursor for TiO_2 and Fe-doped TiO_2 photocatalysts [18, 25]. The use of ilmenite-derived TiO_2 is attractive because it combines mineral-resource utilization with photocatalyst fabrication. Moreover, residual or controlled iron species originating from ilmenite may influence the optical response, defect structure, and charge-transfer behavior of TiO_2. Properly controlled Fe incorporation can narrow the apparent band gap and improve visible-light activity, whereas excessive Fe species may act as recombination centers. Therefore, rational conversion of ilmenite into TiO_2-based photocatalysts requires careful synthesis and structural control.

Although TiO_2, biochar-supported photocatalysts, and ilmenite-derived titanium oxides have each been investigated, limited attention has been given to the integrated design of

ilmenite-derived TiO_2 supported on sugarcane bagasse biomass carbon for adsorption-assisted photocatalytic degradation of SMX. Such a system offers several advantages: ilmenite provides a low-cost mineral source for TiO_2, sugarcane bagasse supplies a renewable biomass-derived carbon support, and the TiO_2/carbon interface enables synergistic adsorption and photocatalytic degradation. In this work, TiO_2 derived from ilmenite was supported on sugarcane bagasse biomass carbon to construct a sustainable hybrid photocatalyst for the removal of SMX from aqueous solution. The prepared composite was characterized in terms of crystalline structure, morphology, surface chemistry, optical properties, and textural features. Its performance was evaluated under dark adsorption and light irradiation to clarify the respective and combined contributions of adsorption, photolysis, and photocatalysis. The degradation kinetics, recyclability, and possible reaction mechanism were also discussed. This study provides a resource-oriented route for developing low-cost TiO_2/carbon photocatalysts from natural mineral and agricultural biomass precursors for the treatment of antibiotic-contaminated water.

Experimental Section

Materials

Ilmenite ore was used as the titanium source. Sugarcane bagasse was collected from a sugarcane juice processing site in Hanoi, Vietnam, washed thoroughly with tap water and deionized water, and dried before use. Potassium bisulfate ($KHSO_4$), sulfuric acid (H_2SO_4), hydrochloric acid (HCl), sodium hydroxide (NaOH), ethanol, and sulfamethoxazole ($C_{10}H_{11}N_3O_3S$) were of analytical grade and used without further purification. Deionized water was used in all synthesis and photocatalytic experiments.

Preparation of TiO_2 precursor from ilmenite ore

The Ti precursor was prepared from ilmenite ore through a sulfate roasting-leaching route. Briefly, ilmenite ore was mixed with $KHSO_4$ at a mass ratio of 1:7 and calcined at 600°C for 2 h in air. After cooling, the roasted product was ground and repeatedly washed with deionized water to remove soluble sulfate and iron-containing impurities. The remaining solid

was then dissolved in 5 wt% H_2SO_4 under continuous stirring to obtain a Ti-rich precursor solution. The obtained precursor was used to synthesise TiO_2 [18].

Preparation of activated carbon from sugarcane bagasse

The cleaned sugarcane bagasse was dried at 105°C for 24 h, milled, and sieved. The dried biomass was first carbonized under an Ar atmosphere at 450°C for 2 h with a heating rate of 10°C min^{-1}. The obtained char was chemically activated by impregnation with 10 wt% HCl at a mass ratio of 1:1 for 24 h, followed by filtration and washing with deionized water until neutral pH. The activated precursor was dried at 105 °C and further carbonized at 500 °C for 60 min under N_2 atmosphere. The resulting sugarcane-bagasse-derived activated carbon was ground, sieved, and stored in a desiccator [21].

Synthesis of TiO_2/activated carbon composite

The TiO_2/activated carbon composite was synthesized by coupling ilmenite-derived TiO_2 with sugarcane-bagasse activated carbon. A defined amount of activated carbon was dispersed in the Ti precursor solution under magnetic stirring and ultrasonication to ensure a homogeneous suspension. The pH was slowly adjusted to approximately 8 - 8.5 using dilute NaOH to promote TiO_2 precipitation onto the carbon surface. The mixture was stirred at 80 °C for 4 h, aged overnight, filtered, and washed several times with deionized water and ethanol. The solid product was dried at 105°C and calcined at 750°C for 2 h under an Ar gas or limited-air atmosphere to obtain the TiO_2/activated carbon composite. For comparison, pure TiO_2 and activated carbon were prepared under similar conditions.

Characterization of materials

The crystalline phases of TiO_2, activated carbon, and TiO_2/activated carbon composite were analyzed by X-ray diffraction using Cu Kα radiation. Surface morphology and elemental composition were examined by scanning electron microscopy coupled with energy-dispersive X-ray spectroscopy. Functional groups were identified by Fourier transform infrared spectroscopy in the range of 400-4000 cm^{-1}. The elemental composition and distribution were

157 analyzed by energy-dispersive X-ray spectroscopy (EDX) coupled with SEM. Textural
158 properties, including BET surface area, pore volume, and pore size distribution, were
159 determined from N_2 adsorption-desorption isotherms at 77 K. Optical absorption properties and
160 band gap energy were evaluated by UV-Vis diffuse reflectance spectroscopy.

161 ***Adsorption-assisted photocatalytic degradation of sulfamethoxazole***

162 Photocatalytic experiments were conducted using sulfamethoxazole hydrochloride as
163 the target antibiotic contaminant. In a typical experiment, 50 mL of SMX solution at the desired
164 initial concentration was transferred to a glass reactor, followed by the addition of the catalyst
165 at a fixed dosage. Before irradiation, the suspension was magnetically stirred in the dark for 60
166 min to establish adsorption-desorption equilibrium. Photocatalytic degradation was then
167 performed under simulated solar irradiation using a 350 W xenon lamp. At predetermined time
168 intervals, aliquots were withdrawn, centrifuged or filtered through a 0.45 μm membrane, and
169 analyzed by UV-Vis spectrophotometry at 265 nm.

170 The SMX removal efficiency was calculated using:

171 $$Removal\ efficiency\ (\%) = \frac{(C_0 - C_t)}{C_0} \times 100 \quad (1)$$

172 Where C_0 and C_t are the initial and time-dependent SMX concentrations, respectively.
173 Control experiments, including photolysis without a catalyst, dark adsorption with activated
174 carbon, dark adsorption with the composite, and photocatalysis with pure TiO_2, were carried
175 out to distinguish adsorption, photolysis, and photocatalytic contributions.

176 ***Kinetic analysis***

177 The photocatalytic degradation kinetics of SMX were evaluated using pseudo-first-
178 order, pseudo-second-order, Elovich, and Bangham models [26]. The apparent pseudo-first-
179 order rate constant was calculated from the linear relationship between $\ln(C_0/Ct)$ and irradiation
180 time. The fitting quality was evaluated using the correlation coefficient (R^2), and the most
181 suitable kinetic model was selected to clarify the dominant degradation behavior, including
182 surface reaction and pore-diffusion effects.

Radical scavenging experiments

Reactive species trapping experiments were conducted to identify the main active species involved in SMX photodegradation. Isopropanol, benzoquinone, and ammonium oxalate were used as scavengers for hydroxyl radicals (•OH), superoxide radicals ($•O_2^-$), and photogenerated holes (h^+), respectively. Each scavenger was added to the SMX solution before irradiation, and the change in degradation efficiency was compared with the scavenger-free system.

Reusability test

The stability and reusability of the TiO_2/activated carbon composite were evaluated over five consecutive photocatalytic cycles. After each run, the catalyst was recovered by filtration or centrifugation, washed with deionized water and ethanol, dried at 80 °C, and reused under identical experimental conditions. The removal efficiency after each cycle was recorded. The used catalyst was further characterized by SEM, and EDX to assess structural and surface stability after repeated photocatalytic operation.

Results and Discussion

Characterizations

Figure 1 shows the morphological evolution from pristine SBAC to the TiO_2/SBAC composite. The pristine SBAC (Figure 1a,b) exhibits a layered and fibrous carbon framework with relatively smooth surfaces, indicating partial preservation of the original lignocellulosic structure after carbonization and activation. Some grooves and interlayer spaces are visible, which can provide diffusion pathways and adsorption sites for SMX molecules. After TiO_2 incorporation, the TiO_2/SBAC composite (Figure 1c,d) shows a much rougher surface, with numerous TiO_2 nanoparticles and aggregates anchored on the carbon matrix. The high-magnification image confirms that TiO_2 particles are distributed over the SBAC surface rather than forming a separate bulk phase. This intimate contact can improve pollutant adsorption near

photocatalytic sites, suppress TiO_2 aggregation, and facilitate interfacial charge transfer, thereby benefiting adsorption-assisted photocatalytic degradation [21].

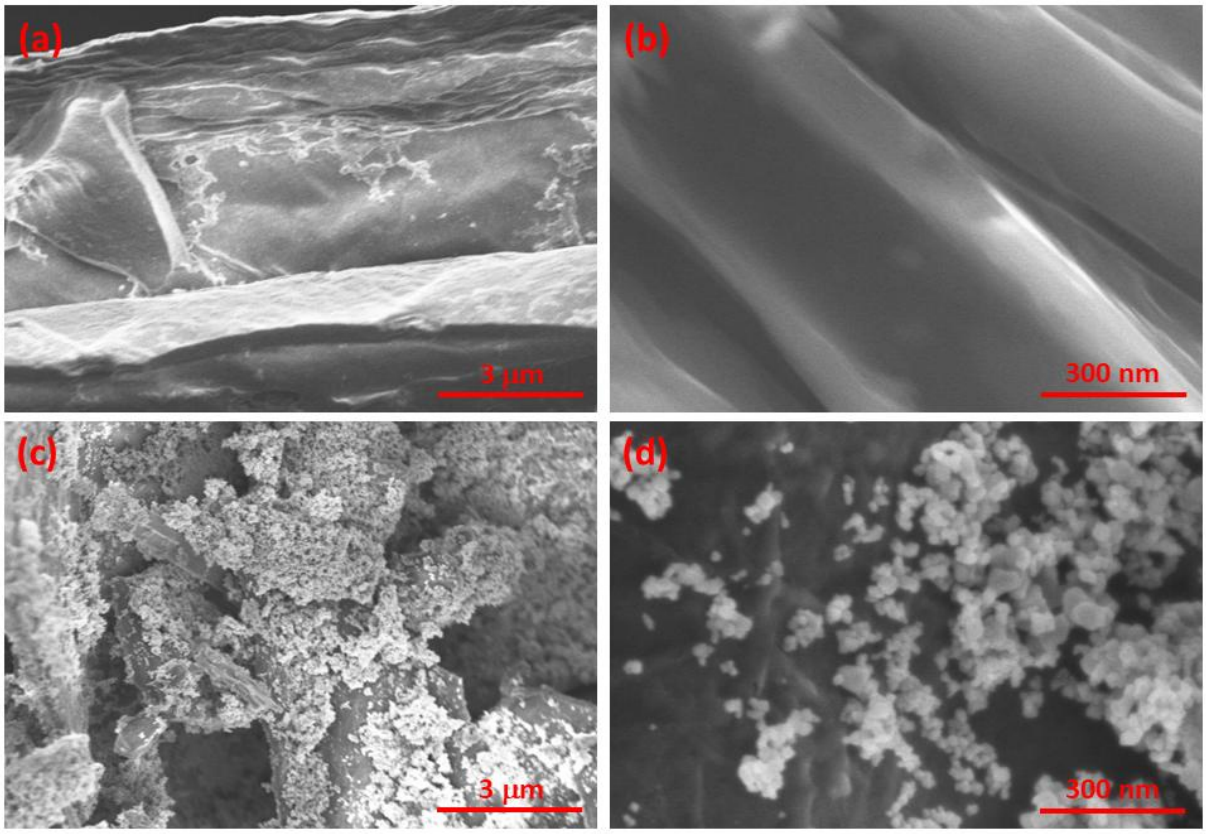
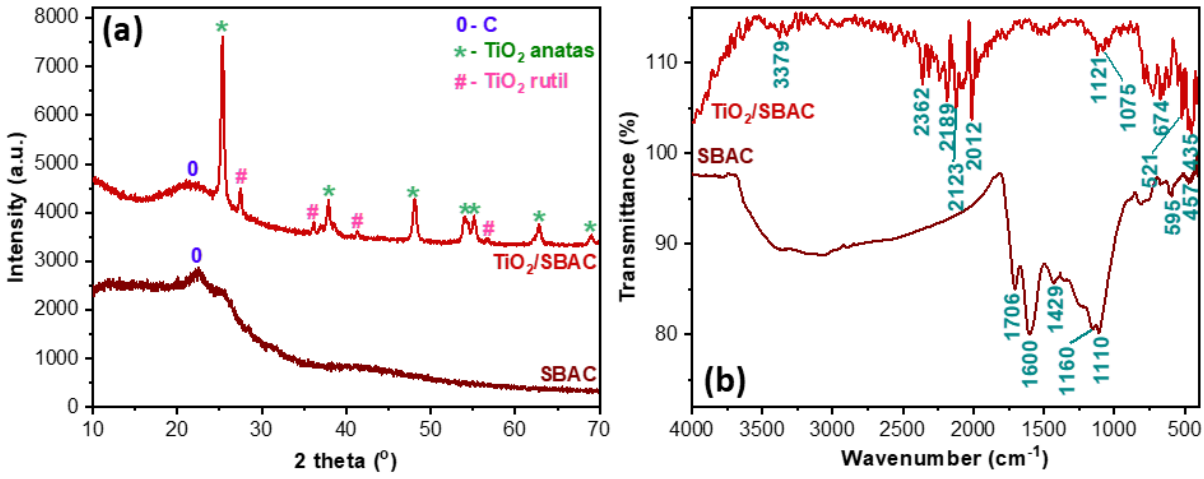


Figure 1. SEM images of sugarcane-bagasse-derived activated carbon (SBAC) and TiO_2/SBAC composite: (a,b) pristine SBAC and (c,d) TiO_2/SBAC composite at low and high magnifications.

Figure 2a shows that pristine SBAC exhibits a broad diffraction band around $2\theta \approx 22$-25°, assigned to disordered graphitic carbon, confirming the largely amorphous structure of biomass-derived activated carbon [21]. After TiO_2 loading, the TiO_2/SBAC composite displays intense diffraction peaks corresponding to anatase TiO_2, together with weaker rutile reflections, indicating successful formation of crystalline TiO_2 on the carbon support [18]. The retained carbon signal suggests that the SBAC framework remains present after composite synthesis. In the FTIR spectra (Figure 2b), SBAC shows bands related to O-H, C=O, aromatic C=C, and C-O/C-O-C groups, confirming oxygen-containing surface functionalities favorable for adsorption. In TiO_2/SBAC, new low-wavenumber bands around 674, 521, and 435 cm^{-1} are attributed to Ti-O and Ti-O-C/Ti-O-Ti vibrations, supporting interfacial interaction between

224 TiO_2 and SBAC. These structural features favor adsorption-assisted photocatalytic SMX
225 degradation [22].
226



227

228 **Figure 2.** (a) XRD patterns and (b) FTIR spectra of SBAC and TiO_2/SBAC composite.

229 Figure 3 presents the EDX spectra and SEM-selected analysis regions of SBAC and
230 TiO_2/SBAC, confirming the compositional change after TiO_2 incorporation. Pristine SBAC is
231 mainly composed of C and O, with minor S and Ca signals, which are likely associated with
232 residual inorganic species and surface functionalities inherited from sugarcane bagasse.
233 Quantitatively, SBAC contains 68.90 wt% C and 29.02 wt% O, confirming a carbon-rich
234 framework with oxygen-containing groups favorable for adsorption (Table 1). After TiO_2
235 loading, the TiO_2/SBAC composite shows clear Ti peaks at approximately 4.5 and 4.9 keV,
236 while C and O remain dominant components. The Ti content reaches 16.25 wt%, confirming
237 successful deposition of TiO_2 on the SBAC matrix. The decrease in C content and increase in
238 O content further support TiO_2 coverage on the carbon surface. These results agree with the
239 SEM observation that TiO_2 particles are anchored on SBAC, forming an integrated
240 photocatalytic-adsorptive composite.

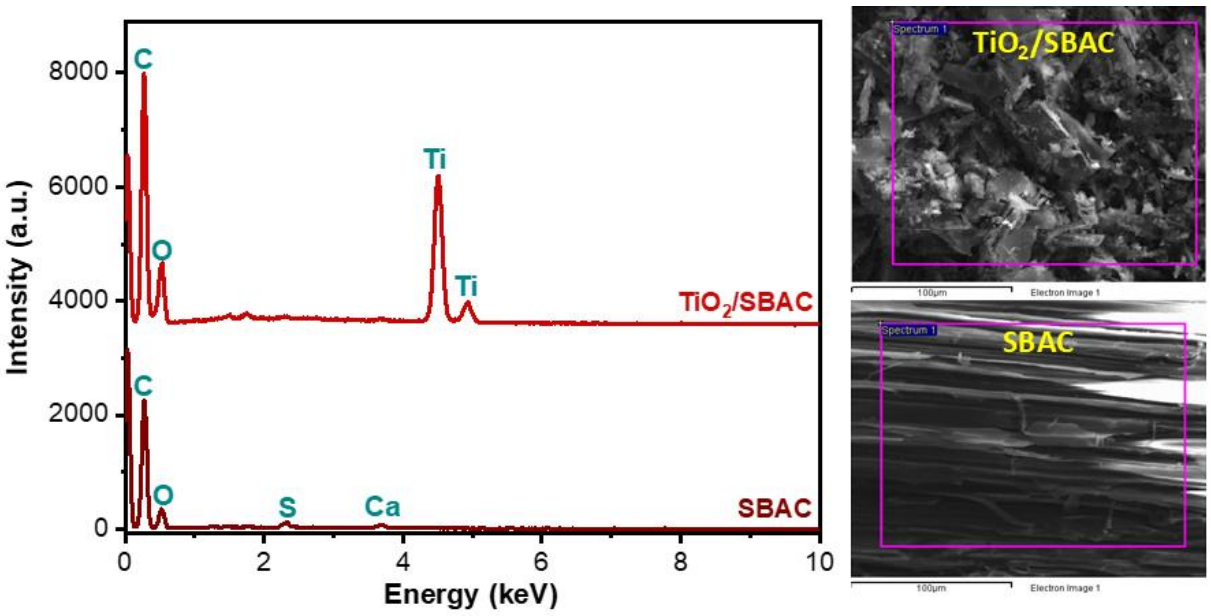


Figure 3. EDX spectra and corresponding SEM analysis areas of SBAC and TiO_2/SBAC composite.

Table 1. Elemental composition of SBAC and TiO_2/SBAC composite determined by EDX analysis.

Element	SBAC		TiO_2/SBAC	
	Weight%	Atomic%	Weight%	Atomic%
C	68.90	75.35	50.50	63.49
O	29.02	23.83	33.25	31.38
Ti	-	-	16.25	5.12
S	1.05	0.44	-	-
Ca	1.03	0.39	-	-
Totals	100.0	100.0	100.0	100.0

Figure 4a presents the N_2 adsorption-desorption isotherms of SBAC and TiO_2/SBAC, both showing mesoporous behavior with clear hysteresis at high relative pressure. Pristine SBAC exhibits a high BET surface area of 473.77 $m^2\ g^{-1}$, pore volume of 0.14 $cm^3\ g^{-1}$, and pore radius of 1.85 nm, confirming its developed porous carbon framework. After TiO_2 deposition,

the BET surface area decreases to 339.39 m^2 g^{-1}, suggesting partial coverage or blockage of carbon pores by TiO_2 particles. However, the pore volume increases to 0.19 cm^3 g^{-1} and the pore radius slightly increases to 1.91 nm, indicating the formation of additional interparticle mesopores within the composite. Figure 4b shows the UV-Vis diffuse reflectance spectrum of TiO_2/SBAC with an absorption edge around 325 nm and an estimated band gap of 3.18 eV, confirming UV-responsive TiO_2 and possible interfacial modification by SBAC.

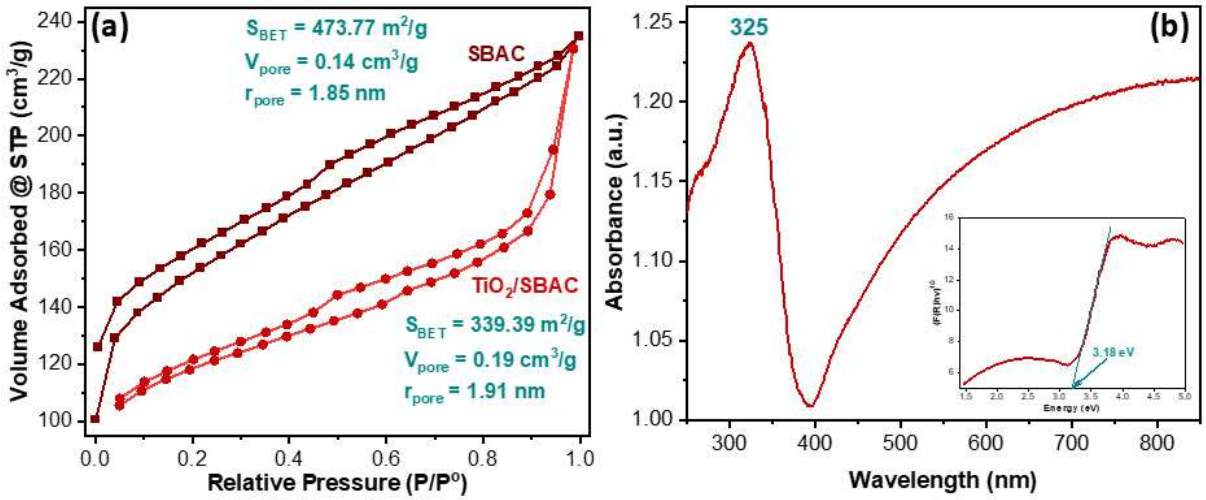


Figure 4. (a) N_2 adsorption-desorption isotherms of SBAC and TiO_2/SBAC composite; and (b) UV-Vis diffuse reflectance spectrum with Tauc plot inset of TiO_2/SBAC.

Adsorption-assisted photocatalytic degradation of sulfamethoxazole (SMX)

Figure 5 compares SMX removal under different reaction conditions, demonstrating the respective contributions of photolysis, adsorption, and photocatalysis. In the absence of catalyst, SMX concentration remains almost unchanged under light irradiation, with only 5.45% removal after 60 min, confirming negligible direct photolysis. Under dark conditions, TiO_2/SBAC removes 54.63% of SMX, whereas SBAC achieves 81.37%, indicating that biomass carbon provides strong adsorption sites, while partial TiO_2 coverage may block some accessible pores and reduce dark adsorption capacity. Pure TiO_2 under light irradiation reaches 90.11% removal, showing its effective photocatalytic activity toward SMX degradation. The TiO_2/SBAC composite under light gives the highest efficiency of 99.46%, with SMX

concentration decreasing almost completely within 60 min. This superior performance confirms an adsorption-assisted photocatalytic mechanism, in which SBAC promotes SMX enrichment and mass transfer, while TiO_2 generates reactive species for oxidative degradation.

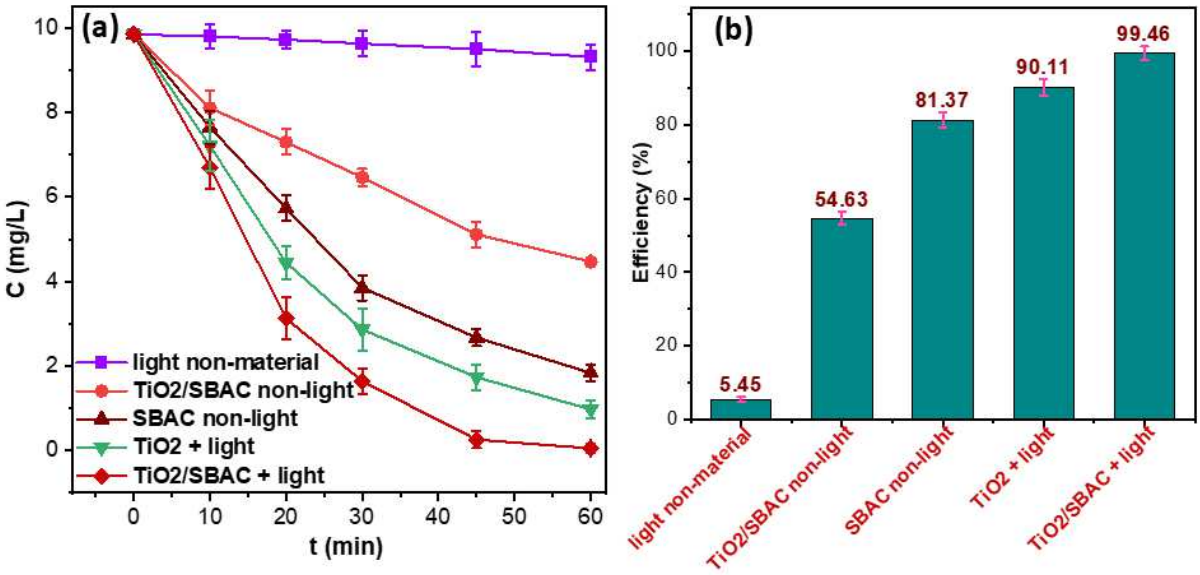


Figure 5. Adsorption-assisted photocatalytic degradation of SMX under different reaction conditions: (a) concentration changes as a function of reaction time and (b) corresponding removal efficiencies after 60 min.

Figure 6 and Table 2 present the Langmuir adsorption isotherm fitting for SMX adsorption on SBAC and TiO_2/SBAC. The SBAC sample shows a moderate linear correlation with $R^2 = 0.904$ and a calculated maximum adsorption capacity of 11.76 mg g^{-1}, suggesting that monolayer adsorption contributes to SMX uptake but is not the only controlling process. This behavior may result from the heterogeneous surface and mixed pore structure of biomass-derived carbon. In comparison, TiO_2/SBAC exhibits a better Langmuir fit with $R^2 = 0.976$ and a much higher q_{max} of 29.41 mg g^{-1}. The increased adsorption capacity indicates that TiO_2 incorporation improves the surface affinity and introduces additional adsorption-active sites for SMX. Therefore, TiO_2/SBAC provides more favorable monolayer adsorption behavior than pristine SBAC, supporting its enhanced adsorption-assisted photocatalytic performance.

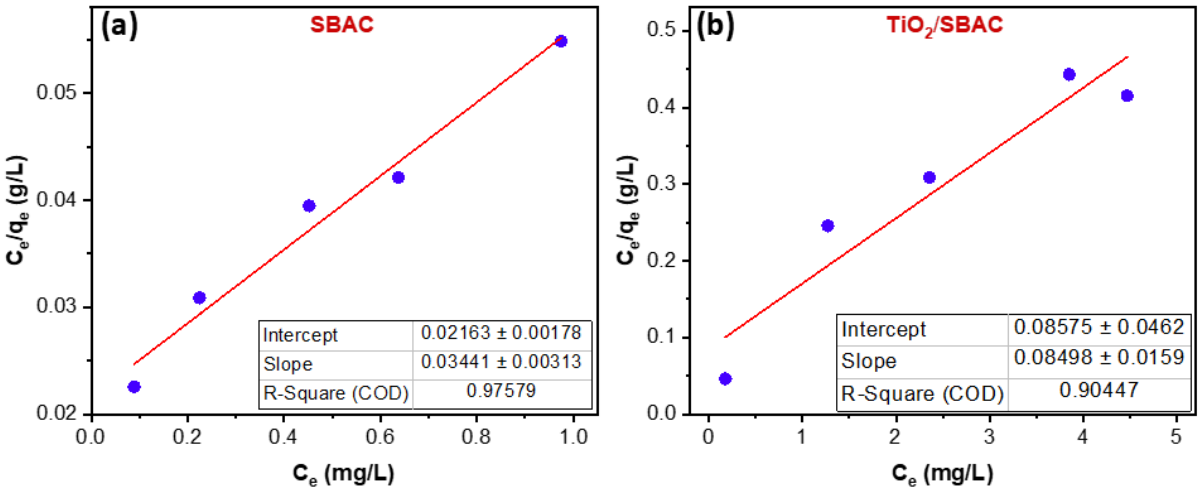


Figure 6. Langmuir adsorption isotherm plots for SMX adsorption on (a) SBAC and (b) TiO_2/SBAC composite.

Table 2. Langmuir isotherm parameters for SMX adsorption on SBAC and TiO_2/SBAC composite.

Material	Slope	q_{max}, mg g^{-1}	R^2
SBAC	0.034	29.41	0.976
TiO_2/SBAC composite	0.085	11.76	0.904

Figure 7 and Table 3 present the kinetic fitting of SMX removal by the TiO_2/SBAC composite using pseudo-first-order, pseudo-second-order, Elovich, and Bangham models. The pseudo-first-order model shows a reasonable fit with $R^2 = 0.949$, $k_1 = 0.085$ min^{-1}, and qe = 13.763 mg g^{-1}, suggesting that concentration-dependent removal contributes to the overall process. The pseudo-second-order model gives a lower correlation coefficient ($R^2 = 0.917$), with $k_2 = 0.0019$ g mg^{-1} min^{-1} and qe = 15.952 mg g^{-1}, indicating that this model is less suitable. The Elovich model provides the best fit, with the highest R^2 value of 0.984, confirming that SMX removal mainly occurs on heterogeneous active sites with variable surface energies. The Bangham model shows the weakest fit ($R^2 = 0.902$), suggesting that pore diffusion contributes but is not the sole rate-controlling step.

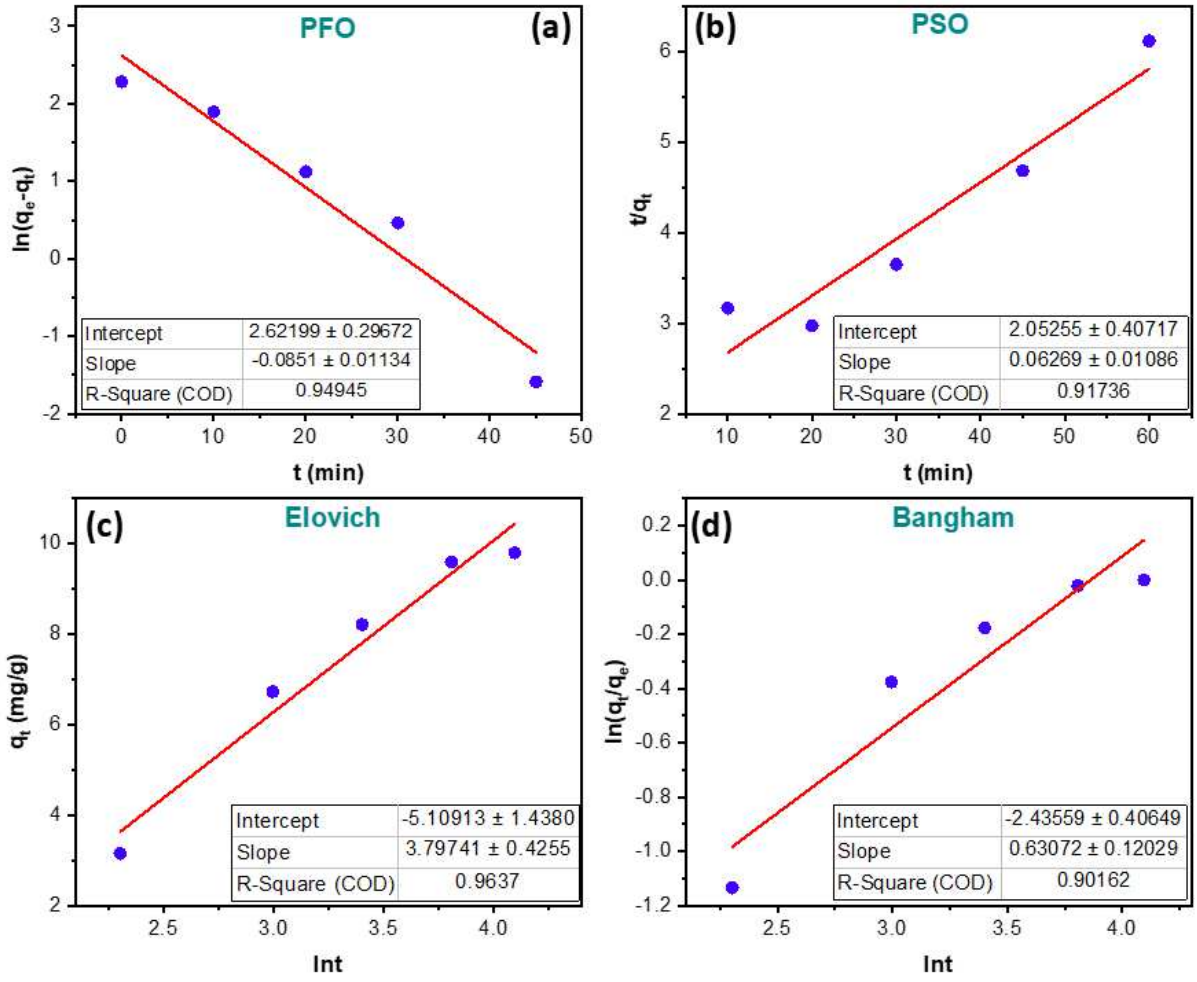


Figure 7. Kinetic fitting plots for SMX removal by TiO_2/SBAC composite using (a) pseudo-first-order, (b) pseudo-second-order, (c) Elovich, and (d) Bangham models.

Table 3. Kinetic parameters for SMX removal by the TiO_2/SBAC composite fitted using pseudo-first-order, pseudo-second-order, Elovich, and Bangham models.

Models	**Parameters**	**Value**	R^2
Pseudo-first order	k_1 (min^{-1})	0.085	0.949
	q_e (mg g^{-1})	13.763	
Pseudo-second order	k_2 (g mg^{-1} min^{-1})	0.0019	0.917
	q_e (mg g^{-1})	15.952	
Elovich	a (mg g^{-1})	0.990	**0.984**
	b (g mg^{-1})	0.263	
Bangham	α	0.631	0.902

	k_B	0.088	

Figure 8a shows the influence of different scavengers on SMX photodegradation over the TiO_2/SBAC composite, clarifying the contribution of reactive species. Without scavenger, SMX degradation reaches nearly 100% after 60 min, confirming the high photocatalytic activity of the composite. The addition of IPA moderately suppresses degradation to about 82%, indicating that •OH radicals participate in SMX oxidation but are not the dominant species. A stronger inhibition is observed with AO, where the efficiency decreases to approximately 73%, suggesting an important role of photogenerated holes in direct oxidation or secondary radical formation. The most pronounced suppression occurs in the presence of BQ, with degradation reduced to about 38%, confirming that $•O_2^-$ radicals are the primary active species. Thus, the reactive species contribution follows the order $•O_2^-$ > h^+ > •OH. Figure 8b shows that TiO_2/SBAC retains good recyclability, with efficiency decreasing from 99.46% to about 86-87% after five cycles, indicating acceptable stability despite slight deactivation due to catalyst loss or surface fouling.

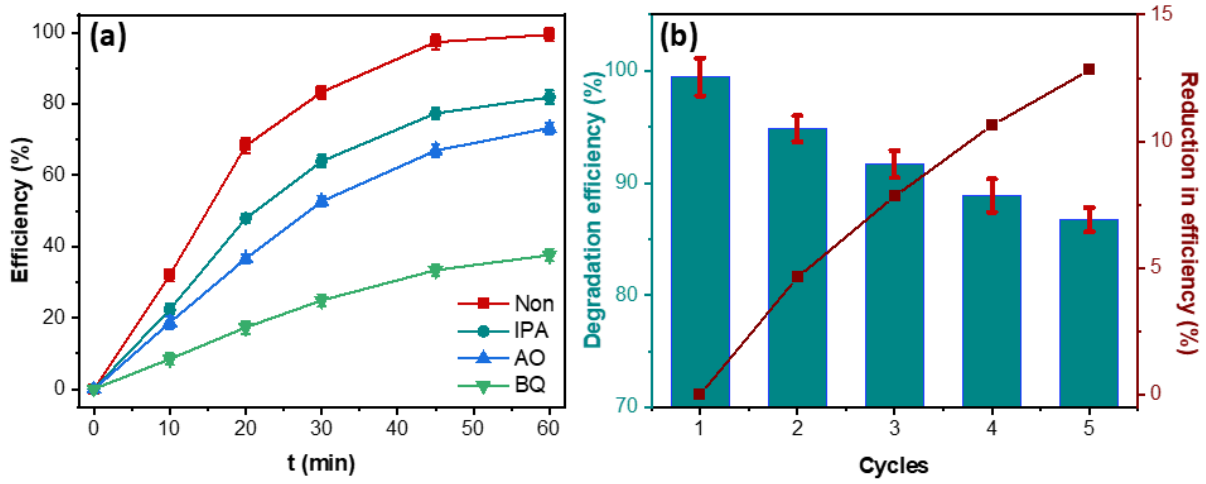


Figure 8. (a) Reactive species trapping experiments for SMX photodegradation over the TiO_2/SBAC composite using IPA, BQ, and AO as scavengers for •OH, $•O_2^-$, and h^+, respectively; and (b) recyclability performance of TiO_2/SBAC over five consecutive cycles.

Figure 9 evaluates the structural and compositional stability of the TiO_2/SBAC composite before and after five photocatalytic degradation cycles. The EDX spectra before and

after reaction show the same major elemental signals of C, O, and Ti, indicating that no obvious elemental loss or impurity deposition occurred during repeated SMX degradation. The elemental composition remains nearly unchanged, with C varying slightly from 50.50 to 50.55 wt%, O from 33.25 to 33.77 wt%, and Ti only decreasing from 16.25 to 15.68 wt%. This small change suggests limited TiO_2 leaching and good compositional stability. SEM images further show that the catalyst retains its rough particle-decorated carbon surface after cycling, although slight aggregation of TiO_2 particles can be observed. The TiO_2/SBAC composite maintains its morphology and elemental integrity, supporting its good reusability and stability.

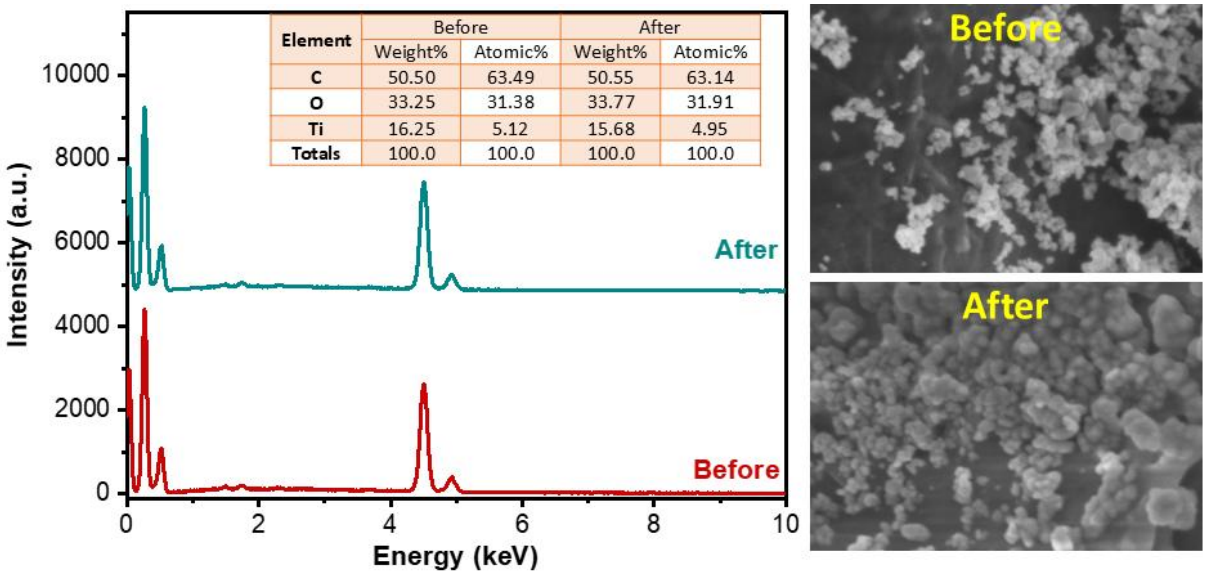


Figure 9. EDX spectroscopy, elemental composition, and SEM images of the TiO_2/SBAC composite before and after photocatalytic degradation of SMX (5 cycles).

The adsorption-assisted photocatalytic degradation of SMX over TiO_2/SBAC can be described as a coupled surface enrichment-photooxidation process. First, SMX molecules are adsorbed onto the porous SBAC surface and near TiO_2 active sites through pore filling, π-π interaction, hydrogen bonding, and electrostatic interaction:

$$SMX(aq) + TiO_2/SBAC \rightarrow SMX\text{-}TiO_2/SBAC(ads) \quad (2)$$

Under light irradiation, TiO_2 is excited to generate electron-hole pairs:

$$TiO_2/SBAC + h\nu \rightarrow TiO_2(e^-CB) + TiO_2(h^+VB)/SBAC \quad (3)$$

The SBAC phase can accept or shuttle photogenerated electrons, suppressing electron-hole recombination:

$$TiO_2(e^-CB) + SBAC \rightarrow TiO_2 + SBAC(e^-) \quad (4)$$

The transferred electrons reduce dissolved oxygen to superoxide radicals:

$$e^-CB/SBAC(e^-) + O_2 \rightarrow \bullet O_2^- \quad (5)$$

Superoxide radicals can further generate hydroperoxyl radicals and hydrogen peroxide:

$$\bullet O_2^- + H^+ \rightarrow \bullet HO_2 \quad (6)$$

$$2\bullet HO_2 \rightarrow H_2O_2 + O_2 \quad (7)$$

$$H_2O_2 + e^- \rightarrow \bullet OH + OH^- \quad (8)$$

Meanwhile, photogenerated holes directly oxidize adsorbed SMX or react with water/hydroxide ions to form hydroxyl radicals:

$$h^+VB + SMX(ads) \rightarrow SMX\bullet^+ \rightarrow \text{degradation intermediates} \quad (9)$$

$$h^+VB + H_2O \rightarrow \bullet OH + H^+ \quad (10)$$

$$h^+VB + OH^- \rightarrow \bullet OH \quad (11)$$

The generated reactive species then attack SMX molecules adsorbed on or near the TiO_2/SBAC surface:

$$SMX(ads) + \bullet O_2^-/\bullet OH/h^+ \rightarrow \text{hydroxylated, oxidized, and ring-opened intermediates} \quad (12)$$

These intermediates are progressively decomposed through cleavage of S-N, C-N, and aromatic ring structures:

$$\text{SMX intermediates} + \bullet O_2^-/\bullet OH/h^+ \rightarrow \text{small organic acids} + NH_4^+/NO_3^- + SO_4^{2-} \quad (13)$$

Finally, deep oxidation may lead to mineralization:

$$\text{small organic acids} + \bullet OH/h^+/O_2 \rightarrow CO_2 + H_2O \quad (14)$$

Overall, the process can be simplified as:

$$SMX + O_2 + H_2O + TiO_2/SBAC + h\nu \rightarrow CO_2 + H_2O + SO_4^{2-} + NO_3^-/NH_4^+ + \text{degradation intermediates} \quad (15)$$

The scavenger experiments support this pathway. The strongest inhibition by BQ indicates that $\bullet O_2^-$ is the dominant reactive species, while the suppression caused by AO confirms the important role of h^+. The weaker inhibition by IPA suggests that •OH participates in SMX oxidation but is not the primary oxidative species. Therefore, the main active species follow the order $\bullet O_2^- > h^+ > \bullet OH$. The superior activity of TiO_2/SBAC is attributed to the adsorption capacity of SBAC, which concentrates SMX near TiO_2, and to interfacial charge transfer, which enhances ROS generation and suppresses electron-hole recombination (Figure 10).

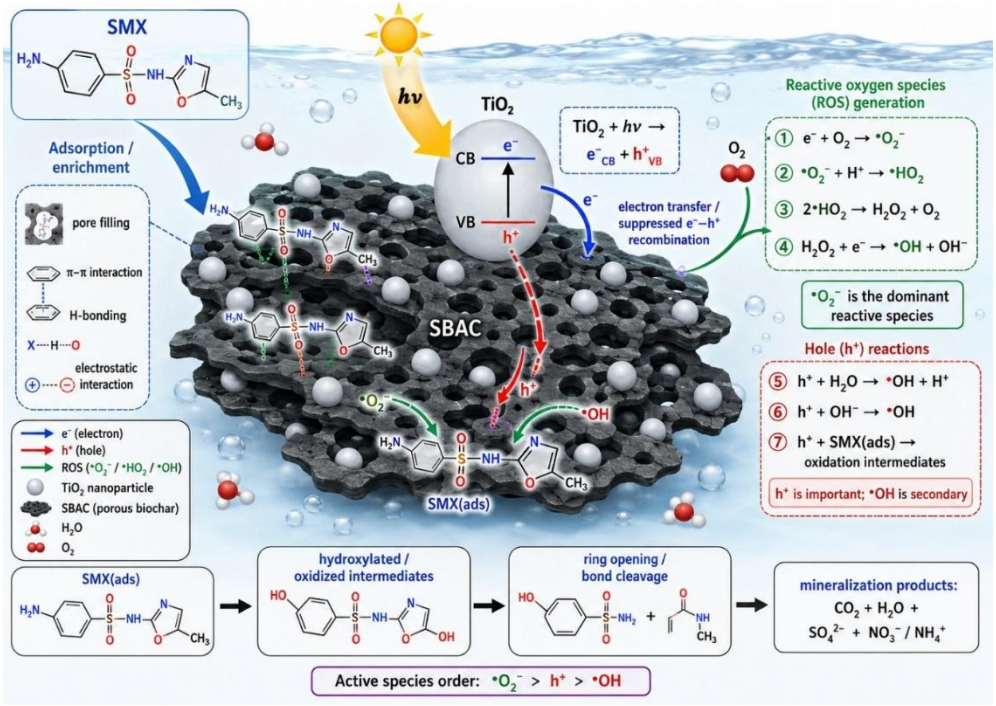


Figure 10. Proposed mechamism for adsorption-assisted photocatalytic degradation of SMX over TiO_2/SBAC.

Table 4 compares representative adsorbents, photocatalysts, and advanced oxidation systems for SMX removal, showing that treatment performance is strongly governed by both material design and removal mechanism. Adsorbent-based systems, especially modified biochars, can exhibit high uptake capacities when pore structure, surface functionality, and activation conditions are optimized. Biosurfactant-modified sludge biochar improves SMX adsorption through altered pore distribution and enriched surface functional groups, while

$ZnCl_2$-activated wheat-straw biochar benefits from abundant micropores that promote pore filling and hydrogen bonding. CO_2-activated biochars derived from leather tannery waste and Sargassum algae also show high Langmuir capacities, with the algae-derived material performing better due to its higher surface area and hierarchical micro-mesoporosity. However, adsorption mainly transfers SMX from the aqueous phase to the solid surface and therefore requires regeneration or subsequent treatment. In contrast, advanced oxidation systems such as MIL-88B(Fe)/H_2O_2/ascorbic acid and Fe^{2+}/dithionite/persulfate can rapidly degrade SMX through reactive oxygen species such as •OH and SO_4•$^-$, but they depend on external oxidants and controlled reaction conditions. Photocatalytic TiO_2-based systems provide oxidative degradation, although their efficiency is often limited by weak adsorption and charge recombination. In this context, the TiO_2/SBAC composite is competitive because it integrates mineral-derived TiO_2 photocatalysis with biomass-carbon-assisted adsorption in a single system. The composite achieved 99.46% SMX removal within 60 min, which is comparable to or higher than several reported advanced oxidation systems. This enhanced performance is attributed to the adsorption-assisted photocatalytic mechanism, in which SBAC concentrates SMX near TiO_2 active sites, promotes interfacial contact, and facilitates charge transfer, thereby enhancing reactive species generation and overall degradation efficiency.

Table 4. Comparison of SMX removal performance using different adsorbents, photocatalysts, and advanced oxidation systems.

Material	**Treatment process**	**Key condition**	**Removal efficiency**	**q_{max} mg g^{-1})**	**Reference**
Biochar-modified iodine-doped TiO_2	Adsorption + photo-degradation	Simulated sunlight, 3 h	40%	-	[14]

Biosurfactant-modified sludge biochar	Adsorption	Batch adsorption	-	43.61	[8]
$CaCl_2$-modified sludge-derived biochar	Adsorption	Batch adsorption	-	22.30	[27]
$ZnCl_2$-activated wheat-straw biochar	Adsorption	pH 5	>90%	315.47	[28]
MIL-88B(Fe)	Fenton-like oxidation	pH 3-9, 60 min	>90%	-	[12]
Fe^{2+}/dithionite	Persulfate oxidation	30 min	84%	-	[29]
FeN-biochar	Electro-assisted persulfate oxidation	Optimized condition	99.67%	-	[30]
Leather-tannery-waste biochar	Adsorption	CO_2 physical activation	-	213	[31]
Sargassum-algae biochar	Adsorption	CO_2 physical activation	-	256.46	[32]

SBAC	Adsorption	Dark condition, 60 min	81.37%	29.41	This study
TiO_2	Photocatalysis	Simulated solar irradiation, 60 min	90.11%	-	
TiO_2/SBAC composite	Adsorption-assisted photocatalysis		99.46%	11.76	

Figure 11 shows the progressive mineralization of SMX during adsorption-assisted photocatalytic degradation over the TiO_2/SBAC composite. The initial TOC value of 4.67 mg L^{-1}, corresponding to the organic carbon content of SMX, decreases rapidly to 3.18 mg L^{-1} after 10 min and further to 1.48 mg L^{-1} after 20 min, indicating efficient breakdown of the parent SMX molecule and partial oxidation of organic intermediates. After 30 min, TOC declines to 0.78 mg L^{-1}, confirming continued degradation of intermediate products. A very low TOC value of 0.12 mg L^{-1} is observed at 45 min, and only 0.03 mg L^{-1} remains after 60 min, corresponding to over 99% TOC removal. These results demonstrate that TiO_2/SBAC not only removes SMX but also enables near-complete mineralization into inorganic end products.

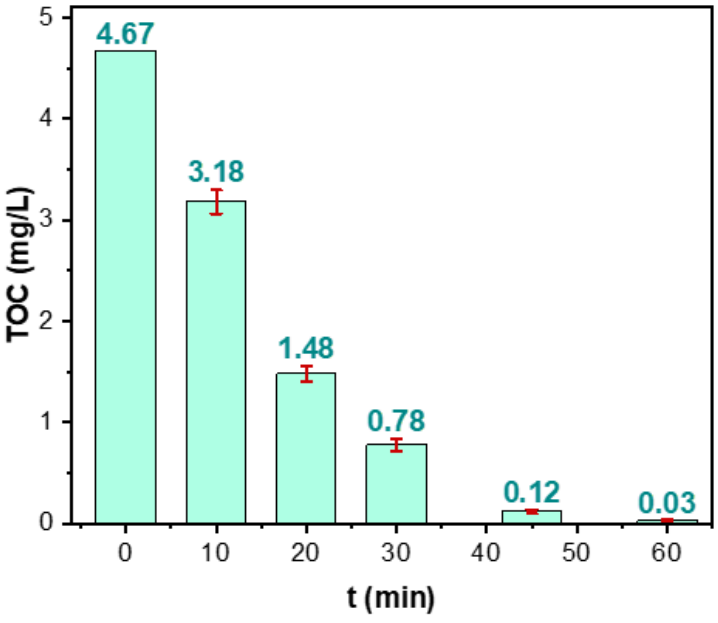


Figure 11. Variation of total organic carbon (TOC) during adsorption-assisted photocatalytic degradation of SMX over the TiO_2/SBAC composite.

Conclusion

This study demonstrated a sustainable route for preparing a TiO_2/SBAC composite from ilmenite ore and sugarcane bagasse biomass carbon for adsorption-assisted photocatalytic degradation of sulfamethoxazole in water. The characterization results confirmed that TiO_2 nanoparticles were successfully anchored on the SBAC surface, forming an integrated porous carbon–semiconductor structure. XRD indicated the presence of anatase and rutile TiO_2 phases, while FTIR, SEM–EDX, BET, and UV–Vis DRS analyses verified the coexistence of surface functional groups, Ti–O-related bonds, mesoporosity, and UV-responsive photocatalytic properties. The TiO_2/SBAC composite achieved 99.46% SMX removal within 60 min under simulated solar irradiation, clearly outperforming direct photolysis, dark adsorption, and individual TiO_2 or SBAC systems. The decrease in TOC from 4.67 to 0.03 mg L^{-1} further confirmed near-complete mineralization rather than simple pollutant transfer. Kinetic fitting followed the Elovich model, suggesting removal on heterogeneous active sites. Radical scavenging experiments revealed that $\bullet O_2^-$ was the dominant reactive species, followed by h^+ and •OH, indicating that electron transfer from TiO_2 to SBAC played a key role in suppressing charge recombination and promoting ROS generation. After five cycles, the catalyst retained about 86.72% degradation efficiency, with only minor changes in morphology and elemental composition. Inconclusion, ilmenite-derived TiO_2 supported on sugarcane bagasse carbon offers a low-cost, resource-oriented, and efficient photocatalytic system for treating antibiotic-contaminated water.

Acknowledgments

This work was supported by the Joint Vietnam-Russia Tropical Science and Technology Research Center under project code MT.Đ1.15/25 on “Research on the fabrication of

TiO_2/TCPP composite materials based on activated carbon from sugarcane bagasse for application in treating some PFOS/PFOA com-pounds in aquatic environment".

Funding

This work was funded by the Joint Vietnam-Russia Tropical Science and Technology Research Center under project code MT.Đ1.15/25

References

[1] S. Li *et al.*, "Linking antibiotic residues and antibiotic resistance genes to water quality parameters in urban reservoirs: a seasonal perspective," *Environments,* vol. 12, no. 3, p. 96, 2025.

[2] I. Beltrán de Heredia, I. Alkorta, C. Garbisu, and E. Ruiz-Romera, "A practical framework for environmental antibiotic resistance monitoring in freshwater ecosystems," *Antibiotics,* vol. 14, no. 8, p. 840, 2025.

[3] J. Liu, T. Wei, X. Wu, H. Zhong, W. Qiu, and Y. Zheng, "Early exposure to environmental levels of sulfamethoxazole triggers immune and inflammatory response of healthy zebrafish larvae," *Science of the total environment,* vol. 703, p. 134724, 2020.

[4] M. Zou *et al.*, "Developmental exposure to environmental levels of sulfamethoxazole (SMX) leads to hyperactivity in zebrafish larvae by inducing oxidative stress and calcium dyshomeostasis," *Journal of Hazardous Materials,* p. 141942, 2026.

[5] K. Krawczyk *et al.*, "Enhanced degradation of sulfamethoxazole by a modified nano zero-valent iron with a β-cyclodextrin polymer: Mechanism and toxicity evaluation," *Science of the Total Environment,* vol. 817, p. 152888, 2022.

[6] Z. Chen *et al.*, "Enhanced sulfamethoxazole removal in water and wastewater by ferrate (VI)/perborate system via borate buffering," *Journal of Hazardous Materials,* vol. 492, p. 138261, 2025.

[7] G. Prasannamedha and P. S. Kumar, "A review on contamination and removal of sulfamethoxazole from aqueous solution using cleaner techniques: Present and future perspective," *Journal of Cleaner Production,* vol. 250, p. 119553, 2020.

[8] T. Zhao, A. Ali, J. Su, S. Liu, H. Yan, and L. Xu, "Removal of sulfamethoxazole from water by biosurfactant-modified sludge biochar: Properties and mechanism," *Journal of Environmental Chemical Engineering,* vol. 12, no. 6, p. 114200, 2024.

[9] H. Liu, F. Xin, X. Wen, H. Zhang, H. Wang, and J. Wei, "Iron and nitrogen co-doped biochar membrane for SMX removal in water by filtration and catalytic oxidation," *Separation and Purification Technology,* vol. 359, p. 130562, 2025.

[10] Y. He *et al.*, "Bio-degraded of sulfamethoxazole by microbial consortia without addition nutrients: mineralization, nitrogen removal, and proteomic characterization," *Journal of hazardous materials,* vol. 466, p. 133558, 2024.

[11] H. Chen and J. Wang, "Degradation of sulfamethoxazole by ozonation combined with ionizing radiation," *Journal of hazardous materials,* vol. 407, p. 124377, 2021.

[12] X. Han *et al.*, "Ascorbic acid promoted sulfamethoxazole degradation in MIL-88B (Fe)/H2O2 Fenton-like system," *Journal of Environmental Chemical Engineering,* vol. 11, no. 1, p. 109144, 2023.

[13] W. Song *et al.*, "Accelerate sulfamethoxazole degradation and detoxification by persulfate mediated with Fe2+ &dithionite: Experiments and DFT calculation," *Journal of Hazardous Materials,* vol. 436, p. 129254, 2022.

[14] Y.-D. Dai, J.-H. Lin, C.-H. Hung, and C. Yuan, "Enhanced removal of sulfamethoxazole via adsorption and photodegradation using biochar-modified iodine-doped TiO2 photocatalysts under simulated sunlight," *Process Safety and Environmental Protection,* vol. 190, pp. 804-816, 2024.

[15] H. N. C. Dharma *et al.*, "A review of titanium dioxide (TiO2)-based photocatalyst for oilfield-produced water treatment," *Membranes,* vol. 12, no. 3, p. 345, 2022.

[16] J. Auene, V. Uahengo, H. M. Kwaambwa, T. Plessing, and A. Gradel, "Synthesis and Optimization of TiO2 Photocatalyst Using Biomass-Derived Activated Carbon for Photocatalytic Degradation of Methyl Orange," *Photochem,* vol. 6, no. 2, p. 18, 2026.

[17] S. Y. Tee *et al.*, "Structurally and surficially activated TiO 2 nanomaterials for photochemical reactions," *Nanoscale,* vol. 16, no. 39, pp. 18165-18212, 2024.

[18] H. P. N. Thi, D. L. Han, D. X. Luu, M. H. D. Thi, D. D. Nguyen, and D. D. La, "Environmentally sustainable photocatalyst for removal of brominated organic pollutants: La_2O_3-TiO_2 composite from ilmenite ore," *Inorganic Chemistry Communications,* p. 116851, 2026.

[19] N. Sylvere, T. Omar, A. Youness, L. El Farissi, and G. Lina, "Innovative applications of sugarcane bagasse in the global sugarcane industry," *Processes,* vol. 13, no. 12, p. 3796, 2025.

[20] M. A. Mahmud and F. R. Anannya, "Sugarcane bagasse-A source of cellulosic fiber for diverse applications," *Heliyon,* vol. 7, no. 8, 2021.

[21] T. T. H. Nguyen *et al.*, "High adsorption capacity of Rhodamine B dye on bio-activated carbon derived from sugarcane bagasse," *Journal of Tropical Science and Engineering,* vol. 1, no. 1, pp. 62-77, 2026.

[22] J. Liu *et al.*, "TiO2/p-BC composite photocatalyst for efficient removal of tetracycline from aqueous solutions under simulated sunlight," *Catalysts,* vol. 14, no. 6, p. 357, 2024.

[23] F. Petronella, A. Truppi, M. Dell'Edera, A. Agostiano, M. L. Curri, and R. Comparelli, "Scalable synthesis of mesoporous TiO2 for environmental photocatalytic applications," *Materials,* vol. 12, no. 11, p. 1853, 2019.

[24] D. Nematov, A. Ashurov, and M. Umarzoda, "Titanium dioxide and photocatalysis: A detailed overview of the synthesis, applications, challenges, advances and prospects for sustainable development," 2024.

[25] J. E. Silveira, V. G. Garcia, L. T. Pacheco, W. S. Paz, J. A. Casas, and J. A. Zazo, "FeTiO3: A low-cost and efficient photocatalytic mineral for sustainable NOx abatement," *Separation and Purification Technology,* vol. 357, p. 130217, 2025.

[26] H. P. N. Thi, T. T. Vuong, P. A. Cao, H. P. N. Thi, and D. D. La, "Hierarchically porous carbon from coffee husk: Pore development and antibiotic adsorption behavior," *Desalination and Water Treatment,* vol. 326, p. 101802, 2026.

[27] Y. Zhou *et al.*, "Recent progress in sludge-derived biochar and its role in wastewater purification," *Sustainability,* vol. 16, no. 12, p. 5012, 2024.

[28] L. Wang, R. Bai, Y. Tian, C. Yang, and X. Tian, "ZnCl2 activation tailoring microporous architecture in wheat straw-derived biochar for enhanced sulfamethoxazole adsorption," *Journal of Water Process Engineering,* vol. 77, p. 108617, 2025.

[29] X. Chen, Y. Zhu, Y. Zhou, G. Tang, J. Han, and W. Li, "Degradation of Sulfamethoxazole in Secondary Wastewater Based on Persulfate Activated by Citric-Acid-Complexed Ferrous Ion under Sunlight," *Water,* vol. 16, no. 11, p. 1564, 2024.

[30] S. Wang *et al.*, "Iron and nitrogen modified sludge biochar efficiently activated persulfate for mineralization of sulfamethoxazole in groundwater," *Journal of Environmental Chemical Engineering,* vol. 11, no. 6, p. 111319, 2023.

[31] S. Jafarian, S. Taghavi, A. M. Lashkar Bolouk, and M. Signoretto, "Sustainable Adsorption of Antibiotics in Water: The Role of Biochar from Leather Tannery Waste and Sargassum Algae in Removing Ciprofloxacin and Sulfamethoxazole," *Sustainability,* vol. 18, no. 1, p. 280, 2025.

[32] R. Ranguin *et al.*, "Biochar and activated carbons preparation from invasive algae Sargassum spp. for Chlordecone availability reduction in contaminated soils," *Journal of Environmental Chemical Engineering,* vol. 9, no. 4, p. 105280, 2021.